Energy Redistribution Following CO₂ Formation on Cold Amorphous Solid Water

Meenu Upadhyay and Markus Meuwly *

Department of Chemistry, University of Basel, Basel, Switzerland

The formation of molecules in and on amorphous solid water (ASW) as it occurs in interstellar space releases appreciable amounts of energy that need to be dissipated to the environment. Here, energy transfer between CO_2 formed within and on the surface of amorphous solid water (ASW) and the surrounding water is studied. Following $CO(^1\Sigma^+) + O(^1D)$ recombination the average translational and internal energy of the water molecules increases on the ~ 10 ps time scale by 15–25% depending on whether the reaction takes place on the surface or in an internal cavity of ASW. Due to tight coupling between CO_2 and the surrounding water molecules the internal energy exhibits a peak at early times which is present for recombination on the surface but absent for the process inside ASW. Energy transfer to the water molecules is characterized by a rapid ~ 10 ps and a considerably slower ~ 1 ns component. Within 50 ps a mostly uniform temperature increase of the ASW across the entire surface is found. The results suggest that energy transfer between a molecule formed on and within ASW is efficient and helps to stabilize the reaction products generated.

Keywords: reactive molecular dynamics, amorphous solid water, interstellar chemistry, energy redistribution, CO₂ formation

1 INTRODUCTION

The motion of adsorbates in and on amorphous solid water (ASW) is essential for chemistry at astrophysical conditions. Typically, bulk water is present in the form of ASW which is the main component of interstellar ices. (Hagen et al., 1981). The structure of ASW is usually probed by spectroscopic measurements (Hagen et al., 1981; Jenniskens and Blake, 1994) although interference-based methods have also been employed. (Bossa et al., 2012). ASWs are porous structures characterized by surface roughness and internal cavities of different sizes which can retain molecular or atomic guests. (Bar-Nun et al., 1987). Under laboratory conditions the water ices have been reported to be porous (He et al., 2016; Kouchi et al., 2020) or non-porous (Oba et al., 2009; He et al., 2016; Kouchi et al., 2020) ASW whereas the morphology of ices in the interstellar medium is more debated. (Keane et al., 2001; Kouchi et al., 2021).

The high porosity of ASW (Bossa et al., 2014; Bossa et al., 2015; Cazaux et al., 2015) makes it a good catalyst for gas-surface reactions involving oxygen (Ioppolo et al., 2011a; Romanzin et al., 2011; Chaabouni et al., 2012; Minissale et al., 2013a; Dulieu et al., 2017; Pezzella et al., 2018; Pezzella and Meuwly, 2019; Christianson and Garrod, 2021), hydrogen (Hama and Watanabe, 2013), carbonaceous (Minissale et al., 2013b; Minissale et al., 2016a; Qasim et al., 2020; Molpeceres et al., 2021) and nitrogen-containing (Minissale et al., 2014) species and helps maintaining those species on (Minissale et al., 2019) or inside ASW. (Minissale et al., 2016b; Tsuge et al., 2020). This

increases the probability for the reaction partners to diffuse to locations for collisions and association reactions to occur. As the diffusivity of individual atoms and small molecules has been established from both, experiments and simulations, (Minissale et al., 2013b; Lee and Meuwly, 2014; Pezzella et al., 2018), this is a likely scenario for formation of molecules on and within ASW.

Earlier thermoluminescence experiments suggested that the $O(^3P)+CO(^1\Sigma^+)$ reaction with both reaction partners in their electronic ground state yields excited CO_2^* which, after emission of a photon, leads to formation of CO_2. (Fournier et al., 1979). Such a process has also been proposed to occur on interstellar grains (Ruffle and Herbst, 2001) and has been confirmed experimentally (Minissale et al., 2013b) with an estimated entrance barrier of 0.014–0.103 eV for the process on ASW, compared with a value of 0.3 eV from high-level electronic structure calculations. (Veliz et al., 2021). The surrounding water matrix provides the necessary coupling (Roser et al., 2001) to facilitate relaxation of the $^3A'$ or $^3A''$ states of CO_2 to the $^1A'$ ground state (correlating with linear $^1\Sigma_g^+$). The presence of an entrance barrier for the $O(^3P)+CO(^1\Sigma^+)$ reaction has one led to consider the alternative CO + OH pathway for CO_2 formation. (Watanabe and Kouchi, 2002; Ioppolo et al., 2011b). This was, however, reconsidered to yield the HOCO intermediate in such environments in more recent experiments. (Qasim et al., 2019). Also, the reaction products of the CO + OH reaction have been found to depend on the experimental conditions. (Oba et al., 2010; Noble et al., 2011). As the CO + OH reaction also appears to have a barrier in the entrance channel, (Noble et al., 2011), attention has recently shifted to the HOCO + H reaction for CO_2 formation. (Qasim et al., 2019).

For adsorbed species to react on ASW they need to be able to diffuse. This has been demonstrated from MD simulations with diffusion coefficients and desorption energies consistent with experiments. (Lee and Meuwly, 2014; Ghesquière et al., 2015). Atomic oxygen (Pezzella et al., 2018) on ASW experiences diffusional barriers between E_{dif} = 0.2 kcal/mol and 2 kcal/mol (100–1000 K) compared with values of $E_{dif} = 990^{+530}_{-360}$ K determined from experiments. (Minissale et al., 2016b). For CO, MD simulations reported (Pezzella and Meuwly, 2019) desorption energies between 3.1 and 4.0 kcal/mol (1560–2012 K or 130–170 meV), compared with 120 meV from experiments. (Karssemeijer et al., 2013). It was also found that the CO desorption energy from ASW depends on CO coverage with ranges from E_{des} = 1700 K for low to 1000 K for high coverage (He et al., 2016) which is consistent with the simulations. (Pezzella and Meuwly, 2019). On non-porous and crystalline water surfaces submonolayer desorption energies for CO are 1307 and 1330 K (~ 115 meV), respectively. (Noble et al., 2012). Experimental diffusional barriers range from 350 ± 50 K (Kouchi et al., 2020) to 490 ± 12 K. (He et al., 2018).

As such association reactions are in general exothermic, the energy released needs to be transferred to environmental degrees of freedom for the reaction products to stabilize. This is the quest of the present work which investigates the time scale and degrees of freedom to receive the energy liberated for the $O(^1D)+CO(^1\Sigma^+)$ reaction to form ground state $CO_2(^1\Sigma_g^+)$. The chemical precursors for formation of CO_2 are believed to be carbon monoxide and atomic oxygen and the CO + O reaction has been proposed as a

non-energetic pathway, close to conditions in interstellar environments, for CO_2 formation 20 years ago from experiments involving a water-ice cap on top of CO and O deposited on a copper surface. (Roser et al., 2001). Formation of $CO_2(^1\Sigma_g^+)$ from ground state $CO(^1\Sigma^+)$ and electronically excited $O(^1D)$ is barrierless. The excited atomic oxygen species can, for example, be generated from photolysis of H²O (Stief et al., 1975) which has a radiative lifetime of 110 min (Garstang, 1951). An alternative pathway proceeds₁ via electron-induced neutral dissociation of water into H² + O(D). (Schmidt et al., 2019). In the presence of CO formation of CO² in cryogenic CO/H²O films was observed. (Schmidt et al., 2019).

After recombination $O(^1D)+CO(^1\Sigma^+) \rightarrow CO_2(^1\Sigma_g^+)$ the product is in a highly vibrationally excited state. For it to stabilize, excess internal energy needs to be channeled into the environment which is the ASW. The present work characterizes and quantifies energy relaxation of the $CO_2(^1\Sigma_g^+)$ product into internal and translational degrees of freedom of the surrounding water matrix. First, the methods used are described. Then, results are presented and discussed. Finally, conclusions are drawn.

2 COMPUTATIONAL METHODS

All molecular dynamics (MD) simulations were carried out using the CHARMM suite of programs (Brooks et al., 2009) with provisions for bond forming reactions through multi state adiabatic reactive MD (MS-ARMD). (Nagy and Yosa Reyes, 2014). The simulation system, **Figure 1**, consisted of an equilibrated cubic box of amorphous solid water with dimension 31 × 31 × 31 Å³ containing 1000 water molecules. As all bonds and angles are flexible, the simulations were run with a time step of Δt = 0.1 fs and the non-bonded cutoff was at 13 Å. Simulations were started from an existing, equilibrated ASW structure (Pezzella et al., 2018; Pezzella and Meuwly, 2019; Upadhyay et al., 2021) by adding CO_A and O_B inside (**Figure 1A**) or on top of (**Figure 1B**) ASW.

In the following, the coordinates are the CO stretch r, the separation R between the center of mass of CO_A and O_B and θ is the O_ACO_B angle. In addition, the $C-O_B$ separation will be considered where appropriate. Initial conditions were generated for a grid of angles θ and separations R and simulations were carried out to obtain initial coordinates and velocities for each of the grid points. With constrained CO and O position, first 750 steps of steepest descent and 100 steps Adopted Basis Newton-Raphson minimization were carried out, followed by 50 ps heating dynamics to 50 K. Then, 100 ps equilibration dynamics was carried out. From each of the runs coordinates and velocities were saved regularly to obtain initial conditions for each combination of angle and distance. Production simulations 500 ps or 6 ns in length were then run from saved coordinates and velocities in the NVE ensemble. Data (energies, coordinates and velocities) were saved every 1000 steps for subsequent analysis.

Water was described by a reparametrized, (Burnham et al., 1997; Plattner and Meuwly, 2008), flexible KKY (Kumagai, Kawamura, Yokokawa) model. (Kumagai et al., 1994). The typical water modes that couple in the ~ 2000 cm⁻¹ region
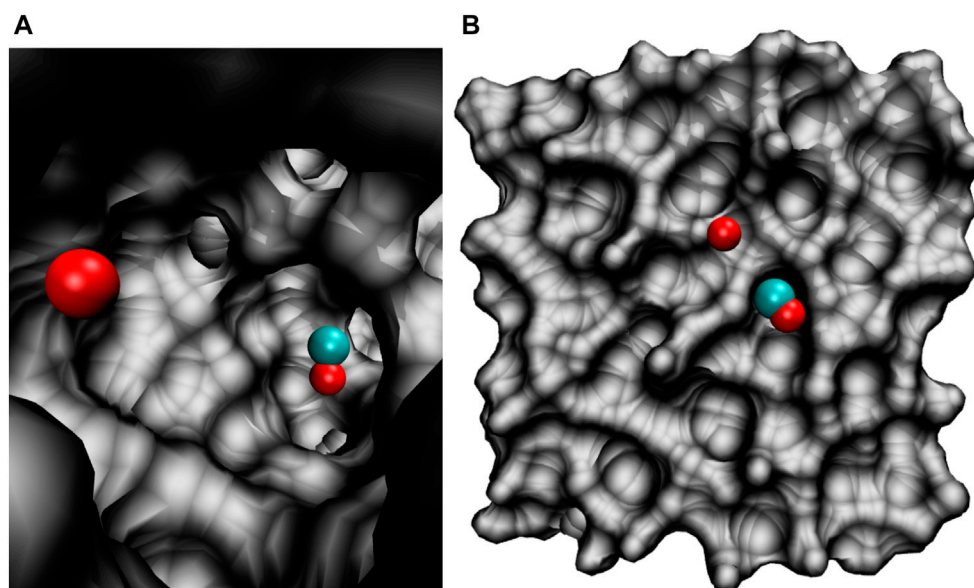
FIGURE 1 | The simulation system for studying the O(^{1}D)+CO($^1\Sigma^+$)→ CO$_2$($^1\Sigma_g^+$) recombination reaction. **(A)**: CO and O trapped inside a cavity of ASW; **(B)**: CO and O on the top of the ASW surface.

relevant in the present work are the water bend (1,600 cm^{-1}) and the framework rotation (600 cm^{-1}) as was also found for the vibrational relaxation of cyanide in water. (Lee and Meuwly, 2011). To describe CO$_A$ + O$_B$ recombination to form CO$_2$ the Morse-Morse-Harmonic (MMH) parametrization was employed. (Upadhyay et al., 2021). This model treats the two CO bonds with a Morse potential and the OCO bend as a harmonic function. MMH is a computationally efficient model (fitted to MRCI/aug-cc-pVTZ data), which yields results for recombination probabilities on ASW comparable to a more elaborate reproducing kernel Hilbert space (RKHS) representation with an exothermicity of −7.27 eV (Veliz et al., 2021; Upadhyay et al., 2021).

For CO$_2$, the partial charges were $q_O = -0.3e$ and $q_C = 0.6e$ with standard van der Waals parameters from CHARMM. These charges are consistent with those obtained from B3LYP/6-31G (d,p) calculations snapshots from the MD simulations with CO$_2$ adsorbed to a small water cluster (H$_2$O)$_{10}$ which yield $q_C = 0.73e$ and $q_O = -0.35e$. This compares with charges of $q_C = 0.22e$ and $q_O = -0.21e$ for the CO molecule and $q_O = -0.1e$ for an oxygen atom adsorbed to (H$_2$O)$_{10}$. To assess the dependence of the results on the partial charges used, additional reactive MD simulations using the MMH parametrization were carried out with $q_O = -0.1e$ and $q_C = 0.2e$ (i.e., $q_{CO} = 0.1e$) and with $q_O = -0.2e$ and $q_C = 0.4e$ (i.e., $q_{CO} = 0.2e$). In all cases, recombination was found to speed up compared with $q_{CO} = 0.3e$ and $q_O = -0.3e$ due to the increased mobility of the CO molecule and the O atom on the ASW when reduced partial charges are used.

The main focus of the present work is to study energy redistribution within the system following recombination of CO$_A$ + O$_B$ to form CO$_2$. For this, the average total, translational and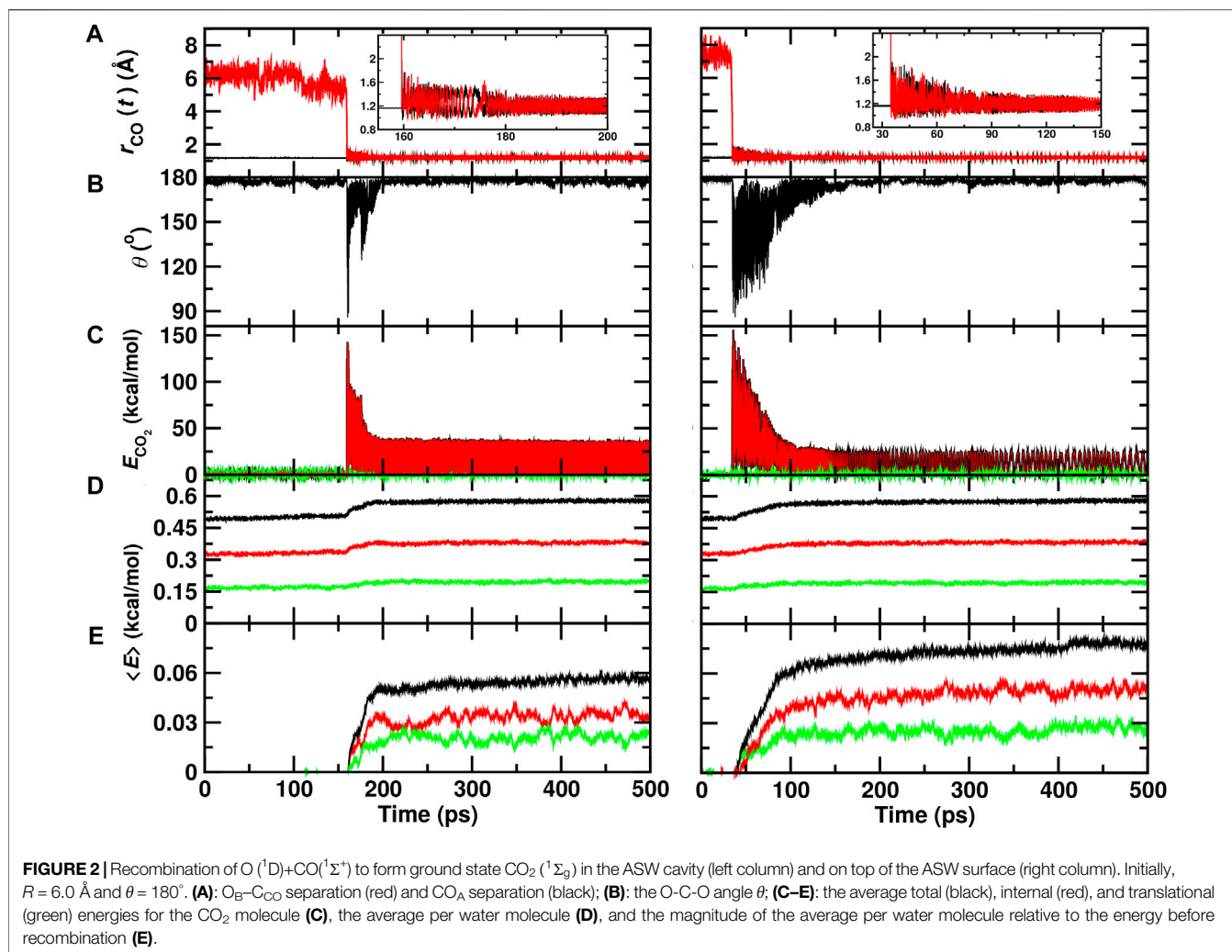 internal energy of the water molecules is analyzed for recombination on top of and inside ASW. Both, the time scale and amount of energy dissipated into translational and internal degrees of freedom was determined. The translational energy for the water molecules at each timestep was determined by first calculating the magnitude of the linear momentum of each water molecule from the stored velocities. From this the translational energy contribution is calculated for each water molecule considered and the total translational energy is accumulated. The internal energy for each water molecule is determined from the difference of the total kinetic energy and the translational energy.

3 RESULTS AND DISCUSSION

In the following, the energy distribution in the water matrix of the ASW is separately discussed on the ~ 100 ps and on the nanosecond time scale. Next, the energy flow away from the recombination site is analyzed and, finally, the energy redistribution to neighboring water molecules surrounding the recombination site is considered.

3.1 Recombination on the 100 ps Time Scale

A typical trajectory for CO$_A$ + O$_B$ recombination inside the ASW cavity is shown in **Figure 2** (left column). Initially, the C–O$_B$ separation is ~ 6 Å (**Figure 2A**). Within 150 ps recombination takes place and angular distortions lead to exploration of angles $\theta_{OCO} \sim 90°$ (**Figure 2B**). Relaxation of the angle occurs within the following 50 ps and the CO$_2$ molecule remains in an internally excited state on much longer time scales, see **Figure 2C**. (Upadhyay et al., 2021). Concomitantly, the average internal energy of the surrounding water molecules increases by about

FIGURE 2 | Recombination of O (^{1}D)+CO($^1\Sigma^+$) to form ground state CO$_2$ ($^1\Sigma_g$) in the ASW cavity (left column) and on top of the ASW surface (right column). Initially, $R = 6.0$ Å and $\theta = 180°$. **(A)**: O$_B$–C$_{CO}$ separation (red) and CO$_A$ separation (black); **(B)**: the O-C-O angle θ; **(C–E)**: the average total (black), internal (red), and translational (green) energies for the CO$_2$ molecule **(C)**, the average per water molecule **(D)**, and the magnitude of the average per water molecule relative to the energy before recombination **(E)**.

10%, see black, red and green traces in **Figures 2D,E**. The translational (phononic) modes (green) acquire approximately 1/3 of the additional energy whereas the internal energy (red) increases by the remaining 2/3.

Figure 2 (right column) reports a recombination trajectory on top of ASW. In this case, recombination takes place after ~ 35 ps and wide angular excursions extend out to 100 ps The amount of energy picked up by the water matrix is larger compared to recombination inside ASW (**Figures 2D,E**). The average total energy per water molecule increases by close to 20% and the amount that goes into internal degrees of freedom is considerably larger. For the translational modes, the energy after recombination is comparable to that for recombination within the cavity.

From a set of 70 recombination trajectories for the reaction within the cavity and on top of the ASW surface, the averaged energy contents in translational, internal and all degrees of freedom of the water molecules were determined (**Figure 3**). For this analysis, the time of reaction was set to zero ($t = 0$) to align all reactive trajectories and all energies are reported relative to the averages before recombination. The translational

contribution for recombination within and on top of ASW re-equilibrates on the ~ 25 ps time scale after which no change in the phononic degrees of freedom is observed. Contrary to that, the internal degrees of freedom (red traces) show temporal evolution on two time scales: a rapid phase on the picosecond time scale, followed by a slow, long increase in the internal energies. This is also reflected in the averaged total energy (black).

As for the single trajectories, the amount of energy released from the recombination reaction into the translational degrees of freedom is similar for the reaction inside the cavity and on top of the ASW surface. For the internal degrees of freedom, however, recombination on top of the ASW surface leads on an average increase per water molecule by 0.075 kcal/mol within 400 ps (**Figure 3B**) compared with 0.06 kcal/mol for the process inside the cavity. Also, there is a characteristic decrease in the internal contribution for recombination on the surface after 15 ps which is even present when averaging over 70 independent runs. This feature is not found for recombination within ASW.

To estimate approximate time scales for the different processes involved, the average energies were fitted to an empirical
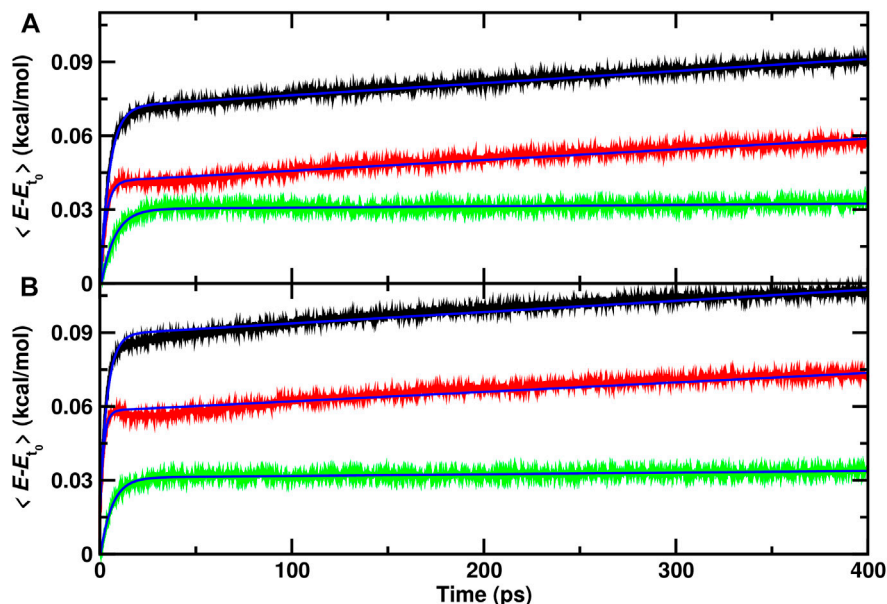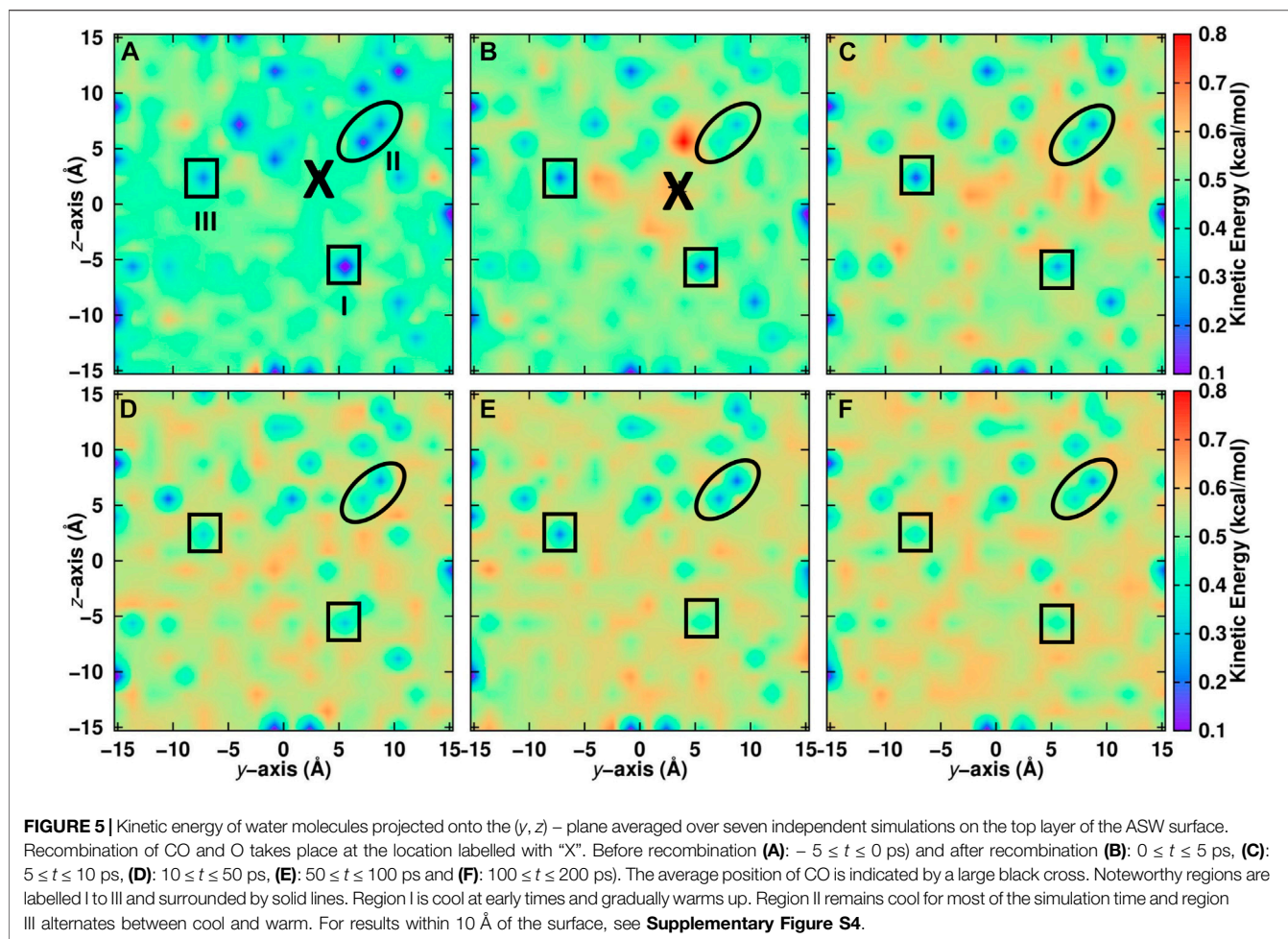
FIGURE 3 | Average total (black), internal (red) and translational (green) energies for water over 70 independent runs relative to the average before recombination. The time of reaction for all trajectories is shifted to $t = 0$ and defined by the first instance at which $r_{C-O_B} < 1.6$ Å. **(A)**: recombination within the ASW cavity. **(B)**: recombination for $CO_A + O_B$ on the top of the ASW surface. The blue solid line is a fit to an empirical expression $\epsilon = a_0 e^{-t/a_1} + a_2 t + a_3$, see text.

expression $\epsilon = a_0 e^{-t/a_1} + a_2 t + a_3$ where ϵ is any of the energies considered. Such a functional form was chosen after inspection of the data in **Figure 3** and accounts for the rapid initial increase in the three energies together with the slow variation of the internal energy on longer times. This parametrization is not able to model

the dip around 15 ps for recombination on to of the surface, though. The time scales a_1 for total, internal, and translational energies are (4.8, 2.9, 7.1) ps for recombination inside the cavity and speed up to (3.9, 1.9, 6.1) ps for the process on the ASW surface. It is of interest to note that the rapid time scale for the
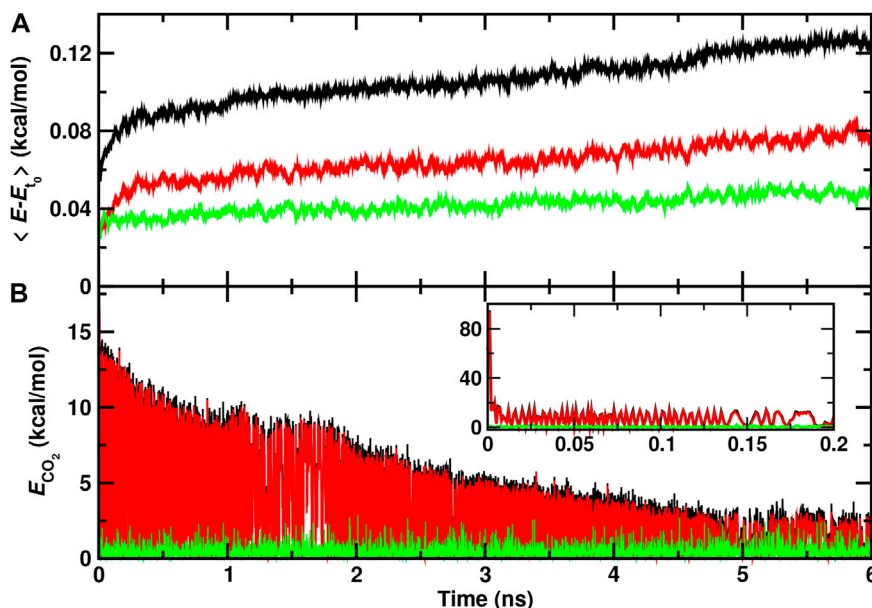
FIGURE 4 | Total (black), internal (red), and translational (green) energies for water molecules **(A)** and for the recombined CO$_2$ molecule **(B)** form a 6 ns rebinding trajectory on the top of the ASW surface. The time of reaction is shifted to $t = 0$ and defined by the first instance at which $r_{C-O_B} < 1.6$ Å. CO$_2$ continues to relax and the energy in the ASW further increases beyond the maximum simulation time of 6 ns after CO$_2$ recombination.

FIGURE 5 | Kinetic energy of water molecules projected onto the (y, z) – plane averaged over seven independent simulations on the top layer of the ASW surface. Recombination of CO and O takes place at the location labelled with "X". Before recombination **(A)**: $-5 \leq t \leq 0$ ps) and after recombination **(B)**: $0 \leq t \leq 5$ ps, **(C)**: $5 \leq t \leq 10$ ps, **(D)**: $10 \leq t \leq 50$ ps, **(E)**: $50 \leq t \leq 100$ ps and **(F)**: $100 \leq t \leq 200$ ps). The average position of CO is indicated by a large black cross. Noteworthy regions are labelled I to III and surrounded by solid lines. Region I is cool at early times and gradually warms up. Region II remains cool for most of the simulation time and region III alternates between cool and warm. For results within 10 Å of the surface, see **Supplementary Figure S4**.

internal energy is considerably faster than the kinetics of the translational degrees of freedom for both types of recombinations. The parameter a_2 which describes the slow increase of internal energy has a value of $a_2 = 4.3 \times 10^{-2}$ (kcal/mol)/ns for recombination in the cavity and $a_2 = 3.8 \times 10^{-2}$ (kcal/mol)/ns for the reaction on the surface, and is vanishingly small for the translational energy.

Average internal energies from representative independent runs for recombination inside the cavity and on top of the ASW surface are shown in **Supplementary Figures S1, S2**. For recombination inside the cavity (**Supplementary Figure S1**) the results confirm that the energy content in the internal degrees of freedom increases considerably faster than for the translation. Also, it is found that the amount of energy transferred to translation after recombination is smaller than that partitioned into internal degrees of freedom. For recombination on the ASW surface the same observations are made. In addition, the pronounced maximum after ~ 5 ps is present in all examples shown in **Supplementary Figure S2**. To provide a molecularly resolved interpretation of this feature the HOH angle time series $\theta(t)$ was analyzed for a trajectory in which CO + O recombination occurred after 35 ps, see **Supplementary Figure S3B**. At the time of reaction the water bending angle decreases from its

average equilibrium value by $\langle \Delta \theta \rangle \sim 1°$ over the next 70 ps after which it relaxes back to the original value. The signature in the internal energy extends over ~ 30 ps, see **Supplementary Figure S2**. Hence, it is possible that changes in the average water geometry following CO + O recombination are responsible for the overshooting and subsequent relaxation of the internal energy for the reaction on the surface. The HOH angle for a simulation within ASW in **Supplementary Figure S3A** also shows a slight adjustment of the valence angle after recombination. Contrary to the situation on the surface, the average angle does not relax to the value before recombination, though.

3.2 Recombination Dynamics on Longer Time Scales

It is also of interest to analyze the energy redistribution on the multi-nanosecond time scale. **Figure 4A** demonstrates that the average total kinetic energy per water molecule continuously increases even on the nanosecond time scale. Most of this increase is due to the internal degrees of freedom although the translational component also shows a continuous slow increase on the nanosecond time scale.
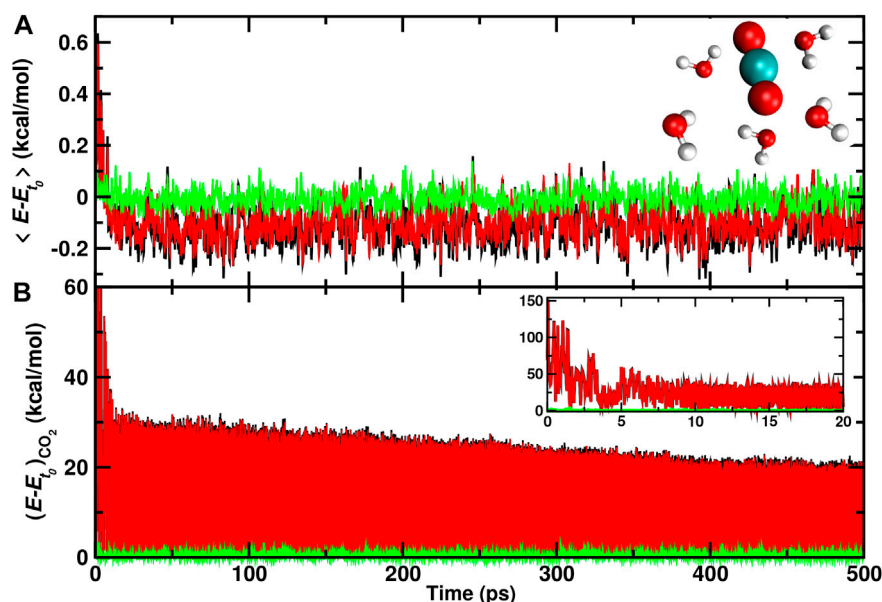
FIGURE 6 | Average total (black), internal (red), and translational (green) energies for 5 water molecules **(A)** closest to the CO$_2$, and the CO$_2$ molecule **(B)** formed from a recombination trajectory on the ASW surface. The time of reaction is shifted to $t = 0$ and defined by the first instance at which $r_{C-O_B} < 1.6$ Å. The initial time scale for energy redistribution from the relaxing CO$_2$ molecule to internal and translational degrees of freedom of the ASW occurs on the 10 ps time scale with slow gradual relaxation on the ~ 100 ps to ns time scale. On the 500 ps time scale the 5 water molecules slightly cool compared with the kinetic energy before recombination.

The relaxation of the CO$_2$ internal energy is reported in **Figure 4B**. Within the first few picoseconds (inset) the internal energy is quenched to ~ 10 kcal/mol after which two relaxations are observed. A first phase during 1 nanosecond following recombination and a second, slower phase extending out to 6 ns and beyond. By the end of the simulation the average internal energy of the CO$_2$ molecule has decreased to ~ 2.5 kcal/mol on average. Hence, it is expected that energy transfer to the surrounding water continues but slows down considerably on the 10 ns time scale and longer.

3.3 Energy Migration Around the Recombination Site

For a positionally resolved picture of energy flow the simulation system was separated in voxels with dimension $31 \times 1 \times 1$ Å^3. The kinetic energy of all water molecules within one such voxel was averaged along the trajectory and projected onto the (y, z) – plane. Which water molecules belong to a particular voxel was decided based on the water-oxygen atom coordinates. **Figure 5A** reports the distribution of total kinetic energy distribution before recombination. The recombination site is at $(y = 2, z = 2)$ Å and marked as a large cross. Within the first 5 ps after recombination the kinetic energy of water molecules within ~ 10 Å of the recombination site increases considerably, by up to a factor of 4. Following this, energy redistributes continuously across the entire surface on the 200 ps time scale, see panels C to F.

Certain regions that are initially "cold" (blue)—e.g., the region labelled "I" at $(y = 5, z = -5)$ Å in **Figure 5**—warm up as energy transfer from CO$_2$ to the water molecules occurs. Conversely, other regions remain "cool", such as region "II" around $(y = 5, z = 5)$ Å for which the color code remains blue until 200 ps. Yet for other regions, such as "III", the total kinetic energy oscillates between cooler and warmer. It is also instructive to include only the first few ASW layers in this analysis which was done in **Supplementary Figure S4**. Here, the voxels have sizes $1 \times 1 \times 1$ Å^3. For one, the cool regions are more extended before recombination. After recombination energy transfer occurs in a similar fashion as for the full system. However, the warm regions are less extended. This suggests that energy transfer also occurs to a considerable extent *into* the bulk rather than across the surface of the ASW even for recombination on top of ASW.

3.4 Energy Flow to Nearby Water Molecules

Finally, individual water molecules in immediate proximity of the recombination site are analyzed. For one trajectory with recombination on the ASW surface the average total, internal, and translational energies for the 5 water molecules closest to the recombination site are reported in **Figure 6**. During the first 10 ps after recombination the average total kinetic energy increases by up to 0.6 kcal/mol per water molecule. Conversely, the translational energy contribution fluctuates around zero which indicates that the local structure of ASW remains intact and most of the energy flows into internal degrees of freedom.

After this initial increase, cooling of these few nearby water molecules takes place with a long-time average of −0.1 kcal/mol

per water molecule in the internal degrees of freedom. On the 500 ps no noticeable change in the translational energy content is observed. For the CO_2 molecule (**Figure 6B**) the translational energy remains small throughout the trajectory whereas the internal energy decreases rapidly within the first 5 ps following recombination. Subsequently, slow gradual cooling on the 100 ps to nanosecond time scale takes place as was already found earlier, **Figure 4**.

4 DISCUSSION AND CONCLUSION

The present work reports on the energy redistribution across ASW following $O(^1D)+CO(^1\Sigma^+)$ recombination to form $CO_2\,(^1\Sigma_g^+)$ on the surface and in a cavity. It is found that energy distribution occurs in two phases, one on the picosecond and one on the nanosecond time scale for both locations. Although the time dependence of the processes is similar for the two different recombination sites (inside vs. on top), the dynamics differs in a number of ways. Firstly, recombination on the surface leads to excess internal energy on the picosecond time scale which subsequently relaxes and additional energy transfer into water modes occurs on longer time scales. Secondly, recombination within the cavity considered here leads to smaller magnitude (∼ 15%) of energy transferred per water molecule compared with the process on the surface (∼ 25%). A possible reason for this is that within a sufficiently large cavity the recombined CO_2 molecule exchanges energy with the surrounding through direct collision whereas on the surface CO_2 is always in contact with the ASW. In other words, the coupling between CO_2 and water differs for recombination within ASW and on top of it. Finally, heating of the water molecules occurs on the 10 ps time scale following the recombination reaction. Consistent with earlier work, (Fredon et al., 2021; Upadhyay et al., 2021), no CO_2 desorption is found from the simulations carried out here.

It is of interest to note that - ultimately - energy redistribution in such systems follows quantum mechanical principles. The present results suggest that the local energy generated from CO + O recombination is probably sufficient to excite internal modes of individual water molecules surrounding the recombination site. Hence, after CO + O recombination the ASW will be in a state characterized by a few internally and vibrationally excited water molecules embedded into a matrix of water molecules in the ground state. Earlier work on a related problem—the vibrational relaxation of a quantum oscillator coupled to oscillators of a biomolecule (Stock, 2009)—found that using classical mechanics leads to qualitatively correct results compared with a full quantum treatment. For the relaxation

times a moderate factor of two for the difference between classical and rigorous quantum simulations was reported. Hence, for the present problem it is also expected that similar conclusions apply and that the nonequilibrium relaxation dynamics of individual vibrationally excited water molecules surrounded by vibrationally cold water molecules can be captured qualitatively from using classical dynamics.

In summary, the present work demonstrates that $O(^1D)+CO(^1\Sigma^+)$ recombination to form $CO_2\,(^1\Sigma_g^+)$ leads to excitation of both, phononic and internal modes of the water molecules that constitute the ASW. The time scales for this are on the pico- and nano-second and lead to warming the water matrix. Water molecules in direct proximity of the recombination site may become vibrationally excited and the time scale for their relaxation back to the ground state will depend on the coupling to the immediate environment. Full relaxation of the CO_2 molecule is expected to require several 10–100 nanoseconds.

DATA AVAILABILITY STATEMENT

The raw data supporting the conclusion of this article will be made available by the authors, without undue reservation. Data on the simulations and the PESs is available at: https://github.com/MMunibas/co2.asw and https://github.com/MMunibas/CO2-PESs.

AUTHOR CONTRIBUTIONS

MM designed research, MU carried out simulations, MU and MM analyzed results, MU and MM wrote manuscript.

SUPPLEMENTARY MATERIAL

The Supplementary Material for this article can be found online at: https://www.frontiersin.org/articles/10.3389/fchem.2021.827085/full#supplementary-material

REFERENCES

Bar-Nun, A., Dror, J., Kochavi, E., and Laufer, D. (1987). Amorphous Water Ice and its Ability to Trap Gases. *Phys. Rev. B* 35, 2427–2435. doi:10.1103/physrevb.35.2427

Bossa, J.-B., Isokoski, K., de Valois, M. S., and Linnartz, H. (2012). Thermal Collapse of Porous Interstellar Ice. *A&A* 545, A82. doi:10.1051/0004-6361/201219340

Bossa, J.-B., Isokoski, K., Paardekooper, D. M., Bonnin, M., van der Linden, E. P., Triemstra, T., et al. (2014). Porosity Measurements of Interstellar Ice Mixtures Using Optical Laser Interference and Extended Effective Medium Approximations. *A&A* 561, A136. doi:10.1051/0004-6361/201322549

Bossa, J.-B., Maté, B., Fransen, C., Cazaux, S., Pilling, S., Rocha, W. R. M., et al. (2015). Porosity and Band-Strength Measurements of Multi-phase Composite Ices. *ApJ* 814, 47. doi:10.1088/0004-637x/814/1/47

Brooks, B. R., Mackerell, A. D., Nilsson, L., Petrella, R. J., Roux, B., Won, Y., et al. (2009). CHARMM: the Biomolecular Simulation Program. *J. Comput. Chem.* 30, 1545–1614. doi:10.1002/jcc.21287

Burnham, C. J., Li, J.-C., and Leslie, M. (1997). Molecular Dynamics Calculations for Ice Ih. *J. Phys. Chem. B* 101, 6192–6195. doi:10.1021/jp9632596

Cazaux, S., Bossa, J.-B., Linnartz, H., and Tielens, A. G. G. M. (2015). Pore Evolution in Interstellar Ice Analogues. *A&A* 573, A16. doi:10.1051/0004-6361/201424466

Chaabouni, H., Minissale, M., Manicò, G., Congiu, E., Noble, J. A., Baouche, S., et al. (2012). Water Formation through O$_2$ + D Pathway on Cold Silicate and Amorphous Water Ice Surfaces of Interstellar Interest. *J. Chem. Phys.* 137, 234706–706. doi:10.1063/1.4771663

Christianson, D. A., and Garrod, R. T. (2021). Chemical Kinetics Simulations of Ice Chemistry on Porous versus Non-porous Dust Grains. *Front. Astro. Space Sci.* 8, 21. doi:10.3389/fspas.2021.643297

Dulieu, F., Minissale, M., and Bockelée-Morvan, D. (2017). Production of O$_2$ through Dismutation of H$_2$O$_2$ during Water Ice Desorption: a Key to Understanding Comet O$_2$ Abundances. *A&A* 597, A56. doi:10.1051/0004-6361/201628445

Fournier, J., Deson, J., Vermeil, C., and Pimentel, G. C. (1979). Fluorescence and Thermoluminescence of N$_2$O, CO, and CO$_2$ in an Argon Matrix at Low Temperature. *J. Chem. Phys.* 70, 5726–5730. doi:10.1063/1.437399

Fredon, A., Radchenko, A. K., and Cuppen, H. M. (2021). Quantification of the Role of Chemical Desorption in Molecular Clouds. *Acc. Chem. Res.* 54, 745–753. doi:10.1021/acs.accounts.0c00636

Garstang, R. H. (1951). Energy Levels and Transition Probabilities in P2 and P4 Configurations. *Monthly Notices R. Astronomical Soc.* 111, 115–124. doi:10.1093/mnras/111.1.115

Ghesquière, P., Mineva, T., Talbi, D., Theulé, P., Noble, J. A., and Chiavassa, T. (2015). Diffusion of Molecules in the Bulk of a Low Density Amorphous Ice from Molecular Dynamics Simulations. *Phys. Chem. Chem. Phys.* 17, 11455–11468. doi:10.1039/c5cp00558b

Hagen, W., Tielens, A. G. G. M., and Greenberg, J. M. (1981). The Infrared Spectra of Amorphous Solid Water and Ice Ic between 10 and 140 K. *Chem. Phys.* 56, 367–379. doi:10.1016/0301-0104(81)80158-9

Hama, T., and Watanabe, N. (2013). Surface Processes on Interstellar Amorphous Solid Water: Adsorption, Diffusion, Tunneling Reactions, and Nuclear-Spin Conversion. *Chem. Rev.* 113, 8783–8839. doi:10.1021/cr4000978

He, J., Acharyya, K., and Vidali, G. (2016). Binding Energy of Molecules on Water Ice: Laboratory Measurements and Modeling. *ApJ* 825, 89. doi:10.3847/0004-637x/825/2/89

He, J., Emtiaz, S., and Vidali, G. (2018). Measurements of Diffusion of Volatiles in Amorphous Solid Water: Application to Interstellar Medium Environments. *ApJ* 863, 156. doi:10.3847/1538-4357/aad227

Ioppolo, S., Cuppen, H. M., and Linnartz, H. (2011). Surface Formation Routes of Interstellar Molecules: Hydrogenation Reactions in Simple Ices. *Rend. Fis. Acc. Lincei* 22, 211–224. doi:10.1007/s12210-011-0135-3

Ioppolo, S., Van Boheemen, Y., Cuppen, H. M., Van Dishoeck, E. F., and Linnartz, H. (2011). Surface Formation of CO$_2$ Ice at Low Temperatures. *Mon. Not. R. Astron. Soc.* 413, 2281–2287. doi:10.1111/j.1365-2966.2011.18306.x

Jenniskens, P., and Blake, D. F. (1994). Structural Transitions in Amorphous Water Ice and Astrophysical Implications. *Science* 265, 753–756. doi:10.1126/science.11539186

Karssemeijer, L., Ioppolo, S., van Hemert, M., van der Avoird, A., Allodi, M., Blake, G., et al. (2013). Dynamics of CO in Amorphous Water-Ice Environments. *Astrophys. J.* 781, 1–15. doi:10.1088/0004-637x/781/1/16

Keane, J. V., Tielens, A. G. G. M., Boogert, A. C. A., Schutte, W. A., and Whittet, D. C. B. (2001). Ice Absorption Features in the 5-8µm Region toward Embedded Protostars. *A&A* 376, 254–270. doi:10.1051/0004-6361:20010936

Kouchi, A., Furuya, K., Hama, T., Chigai, T., Kozasa, T., and Watanabe, N. (2020). Direct Measurements of Activation Energies for Surface Diffusion of CO and CO$_2$ on Amorphous Solid Water Using *In Situ* Transmission Electron Microscopy. *ApJL* 891, L22. doi:10.3847/2041-8213/ab78a2

Kouchi, A., Tsuge, M., Hama, T., Oba, Y., Okuzumi, S., Sirono, S.-i., et al. (2021). Transmission Electron Microscopy Study of the Morphology of Ices Composed of H$_2$O, CO$_2$, and CO on Refractory Grains. *ApJ* 918, 45. doi:10.3847/1538-4357/ac0ae6

Kumagai, N., Kawamura, K., and Yokokawa, T. (1994). An Interatomic Potential Model for H$_2$O: Applications to Water and Ice Polymorphs. *Mol. Simulation* 12, 177–186. doi:10.1080/08927029408022028

Lee, M. W., and Meuwly, M. (2014). Diffusion of Atomic Oxygen Relevant to Water Formation in Amorphous Interstellar Ices. *Faraday Discuss.* 168, 205–222. doi:10.1039/c3fd00160a

Lee, M. W., and Meuwly, M. (2011). On the Role of Nonbonded Interactions in Vibrational Energy Relaxation of Cyanide in Water. *J. Phys. Chem. A.* 115, 5053–5061. doi:10.1021/jp202503m

Minissale, M., Congiu, E., Baouche, S., Chaabouni, H., Moudens, A., Dulieu, F., et al. (2013). Quantum Tunneling of Oxygen Atoms on Very Cold Surfaces. *Phys. Rev. Lett.* 111, 053201. doi:10.1103/PhysRevLett.111.053201

Minissale, M., Congiu, E., and Dulieu, F. (2016). Direct Measurement of Desorption and Diffusion Energies of O and N Atoms Physisorbed on Amorphous Surfaces. *A&A* 585, A146. doi:10.1051/0004-6361/201526702

Minissale, M., Congiu, E., Manicò, G., Pironello, V., and Dulieu, F. (2013). CO$_2$ formation on Interstellar Dust Grains: a Detailed Study of the Barrier of the CO + O Channel. *A&A* 559, A49. doi:10.1051/0004-6361/201321453

Minissale, M., Fedoseev, G., Congiu, E., Ioppolo, S., Dulieu, F., and Linnartz, H. (2014). Solid State Chemistry of Nitrogen Oxides - Part I: Surface Consumption of NO. *Phys. Chem. Chem. Phys.* 16, 8257–8269. doi:10.1039/c3cp54917h

Minissale, M., Moudens, A., Baouche, S., Chaabouni, H., and Dulieu, F. (2016). Hydrogenation of CO-bearing Species on Grains: Unexpected Chemical Desorption of CO. *Mon. Not. R. Astron. Soc.* 458, 2953–2961. doi:10.1093/mnras/stw373

Minissale, M., Nguyen, T., and Dulieu, F. (2019). Experimental Study of the Penetration of Oxygen and Deuterium Atoms into Porous Water Ice. *A&A* 622, A148. doi:10.1051/0004-6361/201833830

Molpeceres, G., Kästner, J., Fedoseev, G., Qasim, D., Schömig, R., Linnartz, H., et al. (2021). Carbon Atom Reactivity with Amorphous Solid Water: H$_2$O-Catalyzed Formation of H$_2$CO. *J. Phys. Chem. Lett.* 12, 10854–10860. doi:10.1021/acs.jpclett.1c02760

Nagy, T., and Yosa Reyes, J. (2014). Multisurface Adiabatic Reactive Molecular Dynamics. *J. Chem. Theor. Comput.* 10, 1366–1375. doi:10.1021/ct400953f

Noble, J. A., Dulieu, F., Congiu, E., and Fraser, H. J. (2011). CO$_2$ Formation in Quiescent Clouds: An Experimental Study of the CO + OH Pathway. *ApJ* 735, 121. doi:10.1088/0004-637x/735/2/121

Noble, J., Congiu, E., Dulieu, F., and Fraser, H. (2012). Thermal Desorption Characteristics of CO, O$_2$ and CO$_2$ on Non-porous Water, Crystalline Water and Silicate Surfaces at Submonolayer and Multilayer Coverages. *Mon. Not. R. Astron. Soc.* 421, 768–779.

Oba, Y., Miyauchi, N., Hidaka, H., Chigai, T., Watanabe, N., and Kouchi, A. (2009). Formation of Compact Amorphous H$_2$O Ice by Codeposition of Hydrogen Atoms with Oxygen Molecules on Grain Surfaces. *ApJ* 701, 464–470. doi:10.1088/0004-637x/701/1/464

Oba, Y., Watanabe, N., Kouchi, A., Hama, T., and Pirronello, V. (2010). Experimental Study of CO$_2$ Formation by Surface Reactions of Non-energetic OH Radicals with CO Molecules. *ApJ* 712, L174–L178. doi:10.1088/2041-8205/712/2/l174

Pezzella, M., and Meuwly, M. (2019). O$_2$ Formation in Cold Environments. *Phys. Chem. Chem. Phys.* 21, 6247–6255. doi:10.1039/c8cp07474g

Pezzella, M., Unke, O. T., and Meuwly, M. (2018). Molecular Oxygen Formation in Interstellar Ices Does Not Require Tunneling. *J. Phys. Chem. Lett.* 9, 1822–1826. doi:10.1021/acs.jpclett.8b00328

Plattner, N., and Meuwly, M. (2008). Atomistic Simulations of CO Vibrations in Ices Relevant to Astrochemistry. *ChemPhysChem* 9, 1271–1277. doi:10.1002/cphc.200800030

Qasim, D., Fedoseev, G., Chuang, K.-J., He, J., Ioppolo, S., van Dishoeck, E. F., et al. (2020). An Experimental Study of the Surface Formation of Methane in Interstellar Molecular Clouds. *Nat. Astron.* 4, 781–785. doi:10.1038/s41550-020-1054-y

Qasim, D., Lamberts, T., He, J., Chuang, K.-J., Fedoseev, G., Ioppolo, S., et al. (2019). Extension of the HCOOH and CO$_2$ Solid-State Reaction Network during the CO Freeze-Out Stage: Inclusion of H$_2$CO. *A&A* 626, A118. doi:10.1051/0004-6361/201935068

Romanzin, C., Ioppolo, S., Cuppen, H. M., van Dishoeck, E. F., and Linnartz, H. (2011). Water Formation by Surface O$_3$ Hydrogenation. *J. Chem. Phys.* 134, 084504–504. doi:10.1063/1.3532087

Roser, J. E., Vidali, G., Manicò, G., and Pirronello, V. (2001). Formation of Carbon Dioxide by Surface Reactions on Ices in the Interstellar Medium. *Astrophys. J. Lett.* 555, L61–L64. doi:10.1086/321732

Ruffle, D. P., and Herbst, E. (2001). New Models of Interstellar Gas-Grain Chemistry - III. Solid CO_2. *Mon. Not. R. Astron. Soc.* 324, 1054–1062. doi:10.1046/j.1365-8711.2001.04394.x

Schmidt, F., Swiderek, P., and Bredehöft, J. H. (2019). Formation of Formic Acid, Formaldehyde, and Carbon Dioxide by Electron-Induced Chemistry in Ices of Water and Carbon Monoxide. *ACS Earth Space Chem.* 3, 1974–1986. doi:10.1021/acsearthspacechem.9b00168

Stief, L. J., Payne, W. A., and Klemm, R. B. (1975). A Flasch Photolysis-Resonance Fluorescence Study of the Formation of O(^{1}D) in the Photolysis of Water and the Reaction of O(^{1}D) with H_2, Ar, and He −. *J. Chem. Phys.* 62, 4000–4008. doi:10.1063/1.430323

Stock, G. (2009). Classical Simulation of Quantum Energy Flow in Biomolecules. *Phys. Rev. Lett.* 102, 118301. doi:10.1103/physrevlett.102.118301

Tsuge, M., Hidaka, H., Kouchi, A., and Watanabe, N. (2020). Diffusive Hydrogenation Reactions of CO Embedded in Amorphous Solid Water at Elevated Temperatures ∼70 K. *ApJ* 900, 187. doi:10.3847/1538-4357/abab9b

Upadhyay, M., Pezzella, M., and Meuwly, M. (2021). Genesis of Polyatomic Molecules in Dark Clouds: CO_2 Formation on Cold Amorphous Solid Water. *J. Phys. Chem. Lett.* 12, 6781–6787. doi:10.1021/acs.jpclett.1c01810

Veliz, J. C. S. V., Koner, D., Schwilk, M., Bemish, R. J., and Meuwly, M. (2021). The C(^{3}P) + O$_2$($^3\Sigma_g^-$) ↔ CO_2 ↔ CO($^1\Sigma^+$)+ O(^{1}D)/O(^{3}P) Reaction: Thermal and Vibrational Relaxation Rates from 15 K to 20000K. *Phys. Chem. Chem. Phys.* 23, 251–263. doi:10.1039/d1cp01101d

Watanabe, N., and Kouchi, A. (2002). Measurements of Conversion Rates of CO to CO_2 in Ultraviolet-induced Reaction of D_2O(H_2O)/CO Amorphous Ice. *ApJ* 567, 651–655. doi:10.1086/338491